ADVANCED MATERIALS
www.advmat.de

www.MaterialsViews.com

Bulk Metallic Glass Composites with Transformation-Mediated Work-Hardening and Ductility

By *Yuan Wu, Yuehua Xiao, Guoliang Chen, Chain T. Liu,* and *Zhaoping Lu**

Bulk metallic glasses (BMGs) have shown a unique combination of mechanical, chemical, and physical properties,[1–5] but their room-temperature brittleness has been the stumbling block for real structural applications.[6,7] To answer this challenge, the concept of developing composite microstructures by combining the glassy matrix with crystalline phases at different length scales has been developed, through which an improvement in tensile ductility has been obtained in several zirconium and titanium-based BMG composites.[8–13] However, these BMG composites showed a macroscopic strain softening phenomenon with an early onset of necking (i.e., the maximum strength occurs at the yield point) because of a lack of work-hardening mechanisms (endows the materials with minute damage tolerance), which would give rise to serious engineering problems therefrom. In this Communication, we report a BMG composite that exhibits large tensile ductility with significant work-hardening capability. Our current finding offers a new paradigm for developing BMGs with improved ductility as practical engineering materials.

A work-hardening phenomenon in compression has been reported in both BMGs and BMG composites and a few scenarios were proposed for understanding the strain-hardening capability, such as severe lattice distortion in the crystalline phases, pile ups of dislocations close to the interfaces between the reinforced phases and matrix,[14] atomic-scale inhomogeneity in the amorphous phase, and stress-induced martensitic transformation.[15–17] To date, however, a working-hardening capability has not been discovered in tension for BMGs or their composites. Referring to the concept of the TRIP (transformation-induced plasticity) steels,[18] in this study, we attempted to fabricate a BMG composite with isolated spherical crystalline phases that undergo martensitic transformation during tensile deformation. With such a special composite structure, large tensile ductility and significant work-hardening capability could be induced.

Figure 1a shows a representative cross section of the current BMG composite, which demonstrates a typical BMG composite microstructure that contains spherical crystalline phases homogeneously embedded in the amorphous matrix. The volume fraction of the crystalline phases is estimated to be about 25%. The high-resolution transmission electron microscopy (HRTEM) image of the spherical crystalline phases shown in Figure 1b suggests an ordered atomic arrangement, and the corresponding selected-area electron diffraction (SAED) pattern in Figure 1c confirms that the crystalline phases are the body-centered cubic (bcc) CuZr phase (i.e., the B2 phase). It is to be noted that B2 particles at the nanoscale can also be found in the amorphous matrix and an example of their morphology is shown in Figure 1d.

Figure 2 illustrates tensile engineering stress–strain curves of the as-cast rods with dimensions as shown in the upper inset. As can be seen, the BMG composite exhibits a distinct tensile behavior from that reported previously for the dendrite-reinforced BMG composites;[8,10] it yielded at about 1280 MPa, followed by a significant increase of the stress (i.e., a strain-hardening process), which can be more clearly demonstrated by the lower inset of the true stress–strain curve. After the maximum tensile strength of about 1650 MPa, the stress started to drop as the strain is further increased, until final fracture. On average, the total tensile ductility of the current BMG composites reaches about 7%.

In order to explore the roles of the B2 phase and related deformation micro-mechanisms, X-ray diffraction (XRD) patterns of the as-cast and fractured samples are compared in **Figure 3a**. The XRD trace of the as-cast specimens is typical for a BMG composite; crystalline phase peaks identified as the B2 phase are superimposed on the amorphous hump, which is consistent with the earlier HRTEM results presented in Figure 1. Nevertheless, the XRD pattern of the fractured samples exhibits different sharp peaks which can be identified as the martensite ZrCu phase (i.e., the B19' phase), suggesting that the martensitic transformation from B2 to B19' has occurred during the tensile deformation. A comparison of the cross-sectional features of the crystalline phases between the as-cast (Figure 3b) and fractured specimens (Figure 3c) provides further evidence for the occurrence of the stress-induced martensitic transition; lath martensite with parallel slats was clearly observed inside the strained spherical crystalline particles. In addition, a similar martensitic morphology was also seen in the nanometer-sized crystals of the fractured samples, as illustrated in Figure 3d. Moreover, a typical SAED pattern of the crystalline phases after the tensile tests is shown in Figure 3e which can be identified as the monoclinic martensitic phase, further verifying the occurrence of the martensitic transformation.

To understand how plastic strains were accommodated and what are the origins of the work hardening during deformation of the current BMG composite, load–unloading experiments were conducted at different deformation stages: right after yielding, work-hardening and stress-drop segment, as indicated by dashed lines in Figure 2. Changes in the lateral surfaces

[*] Dr. Y. Wu, Y. H. Xiao, Prof. G. L. Chen, Prof. Z. P. Lu
State Key Laboratory for Advanced Metals and Materials
University of Science and Technology Beijing
Beijing 100083 (China)
E-mail: luzp@ustb.edu.cn
Prof. C. T. Liu
Mechanical Engineering Department
Hong Kong Polytechnic University
Hung Hom, Kowloon, Hong Kong (China)

DOI: 10.1002/adma.201000482

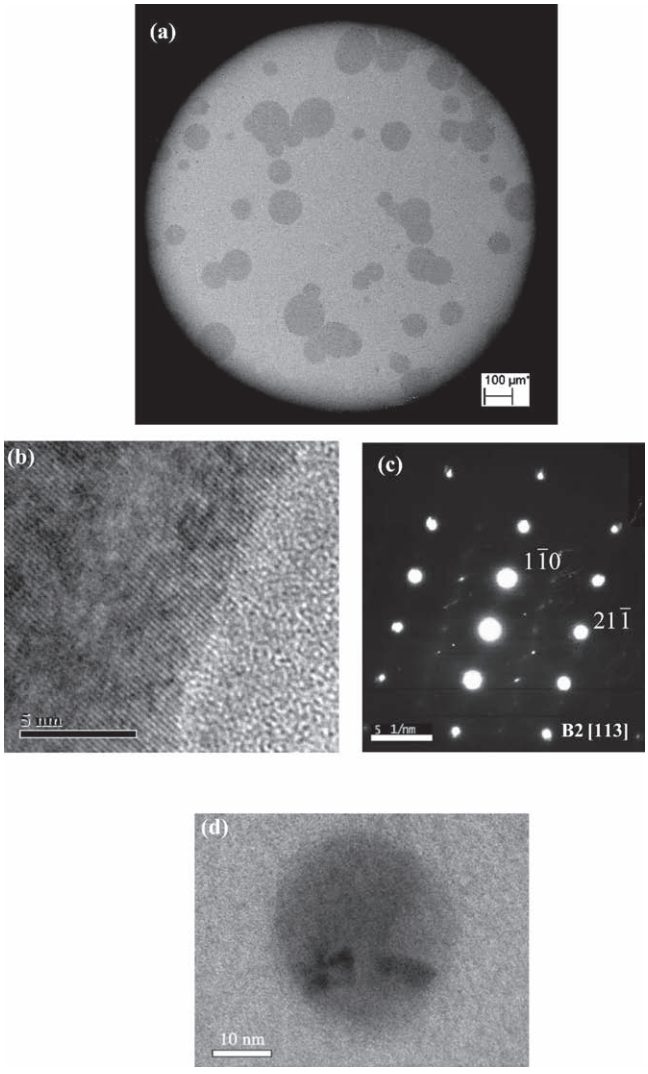

Figure 1. Typical scanning electron microscopy (SEM) image of the cross section of a tensile sample (a). A high-resolution transmission electron microscopy (HRTEM) image of the B2 phase (b) and its selected-area electron diffraction pattern (c). Nanometer-sized B2 phase found in the amorphous matrix (d).

(i.e., along the loading direction) of these strained specimens with increased strain are presented in **Figure 4**. At the beginning of plastic deformation (i.e., right after yielding), the B2 phases are still round but stress concentration is created around their sides as a result of the different responses of the B2 phase and amorphous matrix to the applied stress. Consequently, tiny shear bands start to form from these stress-concentrated sites (Figure 4a). During the work-hardening stage (Figure 4b), the crystalline phases are lengthened along the loading direction and tremendous, tiny shear bands with small spacing are formed. During the stress-drop period, minor cracks have been generated around the oval crystalline phase (see Figure 4c for an example), which are responsible for the stress decrease. This observation suggests that cracks are essentially nucleated at the interfaces where stress concentration is most pronounced, and the fracture is mainly due to separation along the particle–matrix interfaces.

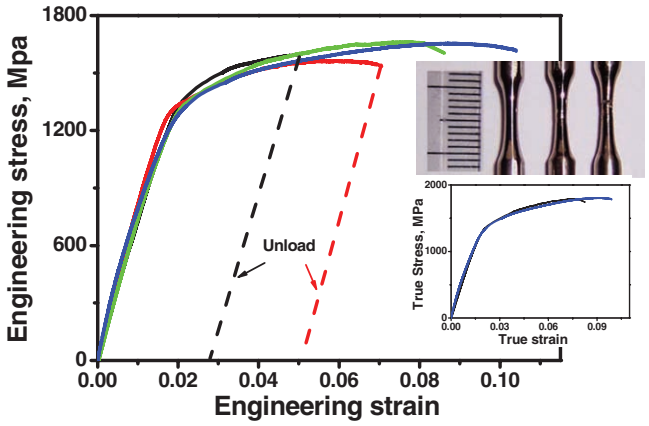

Figure 2. Engineering tensile stress–strain curves of the BMG composites. Dashed lines indicate the unloading process. Top inset shows the outer appearance of the tensile samples pre-strained at the different stages and the lower inset shows the true tensile stress–strain curves, indicating a significant strain-hardening behavior.

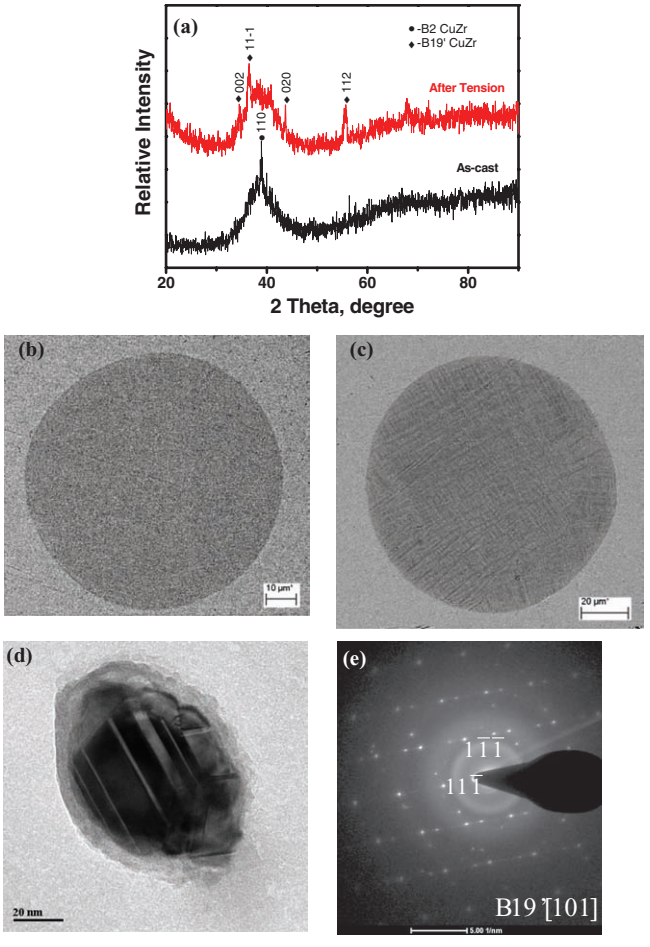

Figure 3. XRD patterns of the as-cast and fractured samples (a). Morphology of the crystalline phase before (b) and after (c) tensile testing. TEM image of the small crystalline phase after tension (d) and an SAED pattern of a transformed crystalline phase (e).

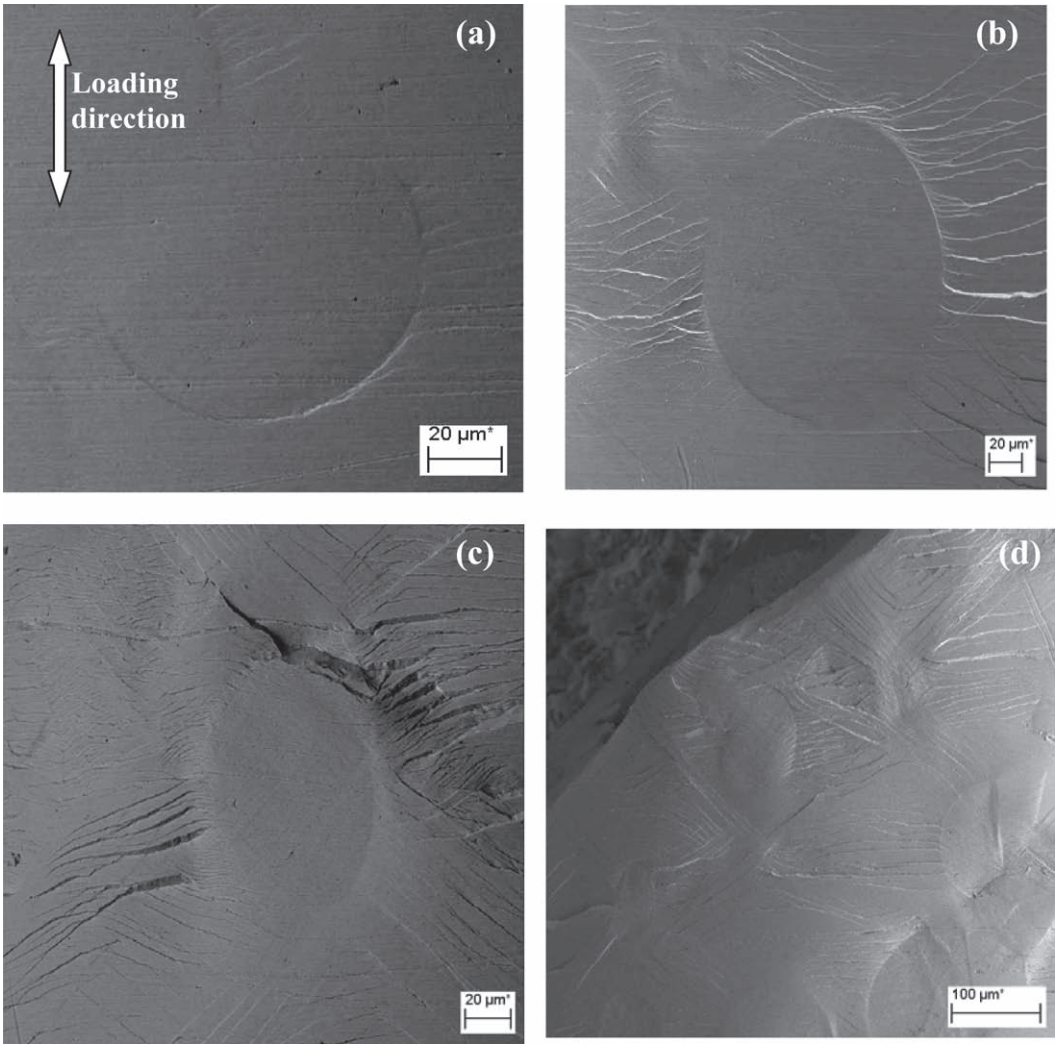

Figure 4. Morphology changes of the crystalline phases during different tensile testing stages: a) just yielded, b) stress increases, c) stress decreases, and d) after fracture.

After fracture (Figure 4d), all the round B2 particles are stretched into oval shapes along the loading direction. It is to be noted that most shear bands are formed perpendicular to the load direction, rather than along the maximum shear-stress direction. The Young's modulus of the B2 phase in the as-cast composite is measured to be 107.3 GPa by nanoindentation, slightly smaller than that of the amorphous matrix (i.e., 108.2 GPa), which enables attraction and/or arrest of shear bands by the crystalline phases, as explained by Hofmann et al.[8,10] As a result, these shear bands would propagate sluggishly and do not easily penetrate the crystalline phases, leading to the extensive shear-band formation, interactions, and multiplication (see Figure 4d). It is necessary to point out that no shear bands around the nanometer-sized crystals were observed, nevertheless, martensitic transformation of these tiny crystals also occurred (Figure 4d) during deformation, which can lead to stress redistribution and contribute to the observed strain hardening.[19]

The hardness variations of the spherical crystalline phases and amorphous matrix for the as-cast and fractured specimens are illustrated in **Figure 5**. It is clear that the spherical crystalline B2 phases are softer than the amorphous phase in the as-cast BMG composite. As the deformation proceeds, the crystalline B2 phase starts to transform into B19' phase and become

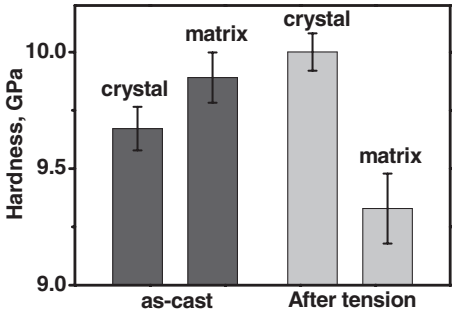

Figure 5. Microhardness of the crystalline phase and amorphous matrix in the as-cast and tensioned samples.

harder and harder while the amorphous matrix is softened due to extensive shear band formation. It is reasonable to rationalize that the observed work hardening is a result of the hardening of the B2 phase. Nevertheless, as demonstrated in the TRIP steels, the back stress effect (i.e., Eshelby effect) from the matrix also plays an important role in the overall strain hardening.[20] Thus, the contribution from the glassy matrix in the current BMG composite can not be ruled out.

As discussed above, the stress-induced martensitic transformation from B2-CuZr to B19'-ZrCu has been observed in the present composite during tension. In the TRIP steels, it has been confirmed that the deformation-induced martensitic transformation can increase the rate of strain hardening and suppress early necking.[18,21] Therefore, it can be speculated that the stress-induced martensitic transformation in the current BMG composite is the controlling mechanism for the observed strain hardening and ductility. To further confirm this hypothesis, another BMG composite with a composition of $Zr_{55}Cu_{29}Ni_8Al_8$ and a similar volume fraction of the Zr_2Cu crystalline phase was synthesized as reported previously.[13] The spherical Zr_2Cu phase does not undergo any transformation during deformation and this specific BMG composite fractured catastrophically without any work hardening or ductility under tension (not shown); this control experiment further verifies that the strain-induced transformation is the main factor for the observed work hardening and large ductility in our present BMG composite. Based on the crack nucleation mode, we expect that the tensile deformation of the composite can be further increased by the enhancement of the B2–matrix interfaces. There is no doubt that further work is required to fully understand the micromechanisms of plastic deformation in the current BMG composites. Nevertheless, the current approach is not believed to be limited to the current BMG composite but also could promote ductility in other BMG systems.

Experimental Section

Alloy ingots with a nominal composition of $Zr_{48}Cu_{47.5}Co_{0.5}Al_4$ [at%] were prepared by arc-melting a mixture of constituent elements with a purity of above 99.9%. Cylinder samples with a diameter of 3 mm and a length of 50 mm were fabricated by suction casting using a copper mold. Tensile samples with a gauge dimension of Φ1.5 mm × 6 mm were then machined and polished from the as-cast rods. Tensile tests were carried out with a WDW-200D machine with a maximum load of 200 kN at an engineering strain rate of 2×10^{-4} s^{-1} and a small strain gauge was used to calibrate and measure the strain during loading. Lateral and cross-sectional surfaces of the as-cast and strained samples were examined in a ZEISS SUPRA 55 scanning electron microscope. Structural characteristics of the as-cast and tested specimens were checked by X-ray diffraction using Cu-K_α radiation and transmission electron microscopy on a JEM 2010F instrument with a field-emission gun. Nanoindentation experiments were conducted to measure the hardness and Young's modulus of the crystal phases and glass matrix by means of an MTS DCM nanoindentation system at a strain rate of 5×10^{-2} s^{-1}.

Acknowledgements

This research was supported by the National Natural Science Foundation of China (No. 50725104) and the 973 program (No. 2007CB613903). Fruitful discussion with Prof. T. G. Nieh at the University of Tennessee is gratefully acknowledged.

Received: February 8, 2010
Revised: March 16, 2010
Published online: April 26, 2010

[1] W. L. Johnson, *MRS Bull.* **1999**, *24*, 42.
[2] A. Inoue, *Acta Mater.* **2000**, *48*, 279.
[3] A. Schuh, T. C. Hufnagel, U. Ramamurty, *Acta Mater.* **2007**, *55*, 4067.
[4] M. F. Ashby, A. L. Greer, *Scripta Mater.* **2006**, *54*, 321.
[5] M. W. Chen, *Annu. Rev. Mater. Res.* **2008**, *38*, 14.
[6] Z. F. Zhang, J. Eckert, L. Schultz, *Acta Mater.* **2003**, *51*, 1167.
[7] F. F. Wu, Z. F. Zhang, S. X. Mao, A. Peker, J. Eckert, *Phys. Rev. B* **2007**, *75*, 134201.
[8] C. Hofmann, J. Y. Suh, A. Wiest, G. Duan, M. L. Lind, M. D. Demetrious, W. L. Johnson, *Nature* **2008**, *451*, 1085.
[9] C. Hays, C. P. Kim, W. L. Johnson, *Phys. Rev. Lett.* **2000**, *84*, 2901.
[10] C. Hofmann, J. Y. Suh, A. Wiest, M. L. Lind, M. D. Demetriou, W. L. Johnson, *Proc. Natl. Acad. Sci. USA* **2008**, *105*, 20136.
[11] G. He, J. Eckert, W. Loser, L. Schultz, *Nat. Mater.* **2003**, *2*, 33.
[12] C. Fan, H. Q. Li, L. J. Kecskes, K. X. Tao, H. Choo, P. K. Liaw, C. T. Liu, *Phys. Rev. Lett.* **2006**, *96*, 145506.
[13] G. Chen, H. Bei, Y. Cao, A. Gali, C. T. Liu, E. P. George, *Appl. Phys. Lett.* **2009**, *95*, 081908.
[14] J. W. Qiao, Y. Zhang, P. K. Liaw, G. L. Chen, *Scripta Mater.* **2009**, *61*, 1087.
[15] J. Das, M. B. Tang, K. B. Kim, R. Theissmann, F. Baier, W. H. Wang, J. Eckert, *Phys. Rev. Lett.* **2005**, *94*, 205501.
[16] K. B. Kim, J. Das, S. Venkataraman, S. Yi, J. Eckert, *Appl. Phys. Lett.* **2006**, *89*, 071908.
[17] S. Pauly, J. Das, J. Bednarcik, N. Mattern, K. B. Kim, D. H. Kim, J. Eckert, *Scripta Mater.* **2009**, *60*, 431.
[18] P. J. Jacques, Q. Fumemont, F. Lani, T. Pardoen, F. Delannay, *Acta Mater.* **2007**, *55*, 3681–3693.
[19] D. V. Louzguine-Luzgin, A. Vinogradov, G. Q. Xie, S. Li, A. Lazarev. S. Hashimoto, A. Inoue, *Philos. Mag.* **2009**, *89*, 2887–2901
[20] K. Tanaka, T. Terasaki, S. Goto, T. Antretter, F. D. Fischer, G. Cailletaud, *Mater. Sci. Eng. A* **2003**, *341*, 189–196.
[21] K. Spencer, J. D. Embury, K. T. Conlon, M. Veron, Y. Brechet, *Mater. Sci. Eng. A* **2004**, *387–389*, 873–881.